J. Fluid Mech. (2010), *vol.* 642, *pp.* 477–487. © Cambridge University Press 2010
doi:10.1017/S0022112009992345

Effect of confinement on three-dimensional stability in the wake of a circular cylinder

SIMONE CAMARRI[1]† AND FLAVIO GIANNETTI[2]

[1]Dipartimento di Ingegneria Aerospaziale, Università di Pisa, via G. Caruso N. 8, 56122 Pisa, Italy

[2]Dipartimento di Ingegneria Meccanica, Università di Salerno, via Ponte don Melillo 1, 84084 Fisciano (Salerno), Italy

(Received 25 May 2009; revised 18 September 2009; accepted 18 September 2009)

This paper investigates the three-dimensional stability of the wake behind a symmetrically confined circular cylinder by a linear stability analysis. Emphasis has been placed on discussing analogies and differences with the unconfined case to highlight the role of the inversion of the von Kármán street in the nature of the three-dimensional transition. Indeed, in this flow, the vortices of opposite sign that are alternately shed from the body into the wake cross the symmetry line further downstream and they assume a final configuration which is inverted with respect to the unconfined case. It is shown that the transition to a three-dimensional state has the same space–time symmetries of the unconfined case, although the shape of the linearly unstable modes is affected by the inversion of the wake vortices. A possible interpretation of this result is given here.

Key words: circular cylinder, confined wake, Floquet analysis, structural sensitivity, three-dimensional stability, von Kármán street

1. Introduction

The flow around a bluff body that is symmetrically confined in a plane channel may show several peculiarities if compared to the unconfined case, and particular attention is paid here to the inversion of the von Kármán street which may take place downstream of the cylinder when alternate vortex shedding from the body occurs. More precisely, vortices are alternately shed in the wake as also in the unconfined case, i.e. if we imagine the flow to be from left to right, clockwise and counterclockwise vortices are shed from the upper and lower sides of the cylinder, respectively. However, at a certain distance along the wake, depending on both the Reynolds number and the blockage ratio, the trajectories of the two families of vortices intersect and, further downstream, their position with respect to the symmetry line is inverted, i.e. counterclockwise and clockwise vortices are positioned in the upper and lower half of the wake, respectively. This phenomenon has been studied in detail for square cylinders in Camarri & Giannetti (2007) and in Suzuki *et al.* (1993) and has been observed for circular cylinders, too (see for instance Rehimi *et al.* 2008; Zovatto & Pedrizzetti 2001); moreover, it continues to exist even when the wake is three-dimensional (see Rehimi *et al.* 2008 or Buffoni *et al.* 2006).

In the authors' opinion, the three-dimensional transition of the wake of a confined bluff body in which the inversion of the von Kármán vortices takes place is extremely

† Email address for correspondence: s.camarri@ing.unipi.it

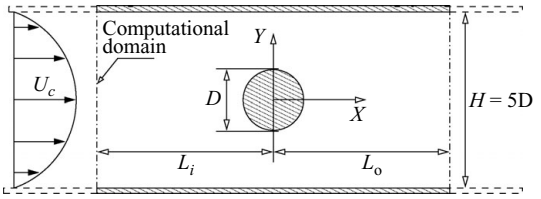

FIGURE 1. Flow configuration, frame of reference and computational domain (not to scale).

interesting to be investigated, as the peculiar configuration of the vortices in this kind of wake might lead to an equally peculiar transition to a three-dimensional state. To the best of the authors' knowledge, the experiments of Rehimi *et al.* (2008) are the only partial investigation of this subject in the literature. They considered a circular cylinder in a channel with a blockage ratio (ratio between the cylinder diameter and the channel height) $\beta = 1/3$. In that case they showed that the transition to a three-dimensional state was characterized by modes similar to those observed in the unconfined case.

In the present work the same flow is considered as a prototype of confined flow with inversion of the wake vortices, but at a more moderate blockage ratio ($\beta = 1/5$), in order to avoid peculiar flow features related to a complex interaction between the wake and the confining walls, as discussed in Camarri & Giannetti (2007). The transition of the considered flow to a three-dimensional state is investigated here by a linear stability analysis, and great emphasis is placed on discussing the analogies and the differences with respect to the unconfined case so as to highlight the role of the vortex inversion in the nature of the transition process. In the unconfined case, two successive types of secondary instabilities have been identified in the classical experiments documented in Williamson (1988, 1996). Those experiments motivated numerical three-dimensional stability analyses of that wake, such as, for instance, those documented in Noack & Eckelmann (1994) or Barkley & Henderson (1996). As concerns the physical nature of the three-dimensional instability of the wake, although an intense debate on the subject still exists in the literature, an interpretation is proposed in Williamson (1996) and is further supported in Thompson, Leweke & Williamson (2001). In particular, these authors suggest that mode A is related to a cooperative elliptic instability of the forming counter-rotating vortices while mode B is caused by an hyperbolic instability of the braid shear layer.

The two-dimensional flow around the configuration considered here has also been investigated in several studies (see for instance Chen, Pritchard & Tavener 1995; Zovatto & Pedrizzetti 2001; Sahin & Owens 2004) and, to the best of the authors' knowledge, its three-dimensional stability limit has never been studied for the considered blockage ratio; this quantitative information is a useful, even if secondary, output of the present analysis.

2. Flow configuration, governing equations and numerical tools

The incompressible flow around an infinitely long circular cylinder, symmetrically confined by two parallel plates with an incoming Poiseuille flow, is considered here. With reference to figure 1 the blockage ratio is $\beta = D/H = 1/5$ and the Reynolds number is defined as $Re = U_c D/\nu$, ν being the kinematic viscosity of the fluid.

The transition of the considered flow from a two-dimensional to a three-dimensional state is investigated by a standard Floquet analysis. In particular, for a given Reynolds number above the critical one for primary instability, the two-dimensional

time-periodic flow field $\boldsymbol{Q}=\{\boldsymbol{U}_b, P_b\}$ (velocity $\boldsymbol{U}_b(t)$ and pressure $P_b(t)$) is computed, T being the corresponding period. A three-dimensional perturbation field $\boldsymbol{q}=\{\boldsymbol{u}, p\}$ is then considered, and its Fourier transform in the homogeneous spanwise direction (z) is assumed to have the following form: $\boldsymbol{q}(x, y, \kappa, t)=\hat{\boldsymbol{q}}(x, y, \kappa, t)\exp(\sigma t)$, where k is the wavenumber in the z direction, $\sigma \in \mathbb{C}$ is the Floquet exponent and $\hat{\boldsymbol{q}}=\{\hat{\boldsymbol{u}}, \hat{p}\}$ is periodic in time with the same period T as the base flow. When the equations governing the dynamics of the disturbance $\boldsymbol{q}$, which is superposed on the base flow $\boldsymbol{Q}$, are linearized and Fourier-transformed in z, the following set of equations is obtained:

$$\frac{\partial \hat{\boldsymbol{u}}}{\partial t}+\sigma\hat{\boldsymbol{u}}+\boldsymbol{U}_b\cdot\nabla_\kappa\hat{\boldsymbol{u}}+\hat{\boldsymbol{u}}\cdot\nabla_\kappa\boldsymbol{U}_b-\frac{1}{Re}\Delta_\kappa\hat{\boldsymbol{u}}+\nabla_\kappa\hat{p}=0, \tag{2.1a}$$

$$\nabla_\kappa\cdot\hat{\boldsymbol{u}}=0, \tag{2.1b}$$

where $\nabla_\kappa \equiv (\partial/\partial x, \partial/\partial y, \mathrm{i}\kappa)$ and $\Delta_\kappa \equiv \nabla_\kappa\cdot\nabla_\kappa$ are the Fourier-transformed gradient and Laplacian operators, respectively. The above equations are completed by homogeneous boundary conditions on the solid walls, appropriate far-field radiation conditions, and the periodicity constraint for $\hat{\boldsymbol{q}}$ in time. The resulting problem is thus an eigenvalue problem. The flow is linearly unstable at a given Reynolds number if at least a non-trivial solution of (2.1) exists, for a particular value of k, such that the norm of the associated Floquet multiplier $\mu=\exp(\sigma T)$ is greater than 1 ($\|\mu\|>1$).

In the following analysis, information coming from the solution of the adjoint equations associated with the system (2.1) is used too. In particular, it is assumed that the form of the flow field adjoint to $\boldsymbol{q}(x, y, k, t)$ is $\boldsymbol{g}^+(x, y, \kappa, t)=\hat{\boldsymbol{g}}^+(x, y, \kappa, t)\exp(-\sigma t)$, where $\hat{\boldsymbol{g}}^+=\{\hat{\mathbf{f}}^+, \hat{m}^+\}$ is periodic in time with the same period T as the base flow. Consequently, the set of equations adjoint to (2.1) has the following form:

$$\frac{\partial \hat{\mathbf{f}}^+}{\partial t}-\sigma\,\hat{\mathbf{f}}^+ + \boldsymbol{U}_b\cdot\nabla_\kappa\hat{\mathbf{f}}^+ - \nabla_\kappa\boldsymbol{U}_b\cdot\hat{\mathbf{f}}^+ + \frac{1}{Re}\Delta_\kappa\hat{\mathbf{f}}^+ + \nabla_\kappa\hat{m}^+=0, \tag{2.2a}$$

$$\nabla_\kappa\cdot\hat{\mathbf{f}}^+=0, \tag{2.2b}$$

with homogeneous boundary conditions on the cylinder surface, appropriate radiation conditions in the far field and the periodicity constraint for $\hat{\boldsymbol{g}}^+$ in time. We refer to Luchini, Giannetti & Pralits (2008) and Giannetti, Camarri & Luchini (2009) for the derivation of (2.2).

The two-dimensional incompressible Navier–Stokes equations, their linearized version (2.1) for three-dimensional perturbations that are periodic in the spanwise direction and the corresponding adjoint equations (2.2) are discretized in space, in conservative form, on a staggered Cartesian mesh by a standard centred and second-order-accurate finite-difference scheme. The cylinder surface is simulated by an immersed-boundary technique that preserves second-order accuracy (see Giannetti & Luchini 2007). For the simulation of the two-dimensional base flow, the velocity field is forced to have a Poiseuille profile at the inflow, while it vanishes on the channel walls, and convective boundary conditions are applied on the outflow boundary. For the simulation of the linearized equations, the velocity field is also forced to vanish at the inflow. The resulting semidiscrete equations are advanced in time by a hybrid third-order Runge–Kutta/Crank–Nicolson scheme. Once discretized, the linearized equations (2.1) (adjoint equations (2.2)) become a discrete eigenvalue problem. The Floquet multipliers have been numerically evaluated in this work by using both a power method and the implicitly restarted Arnoldi method implemented in the ARPACK library. Since in our code we solve the adjoint of the discrete equations (2.1), the Floquet multipliers for the direct and adjoint problems are equal to machine accuracy. All the codes used in the present work have been widely validated in the

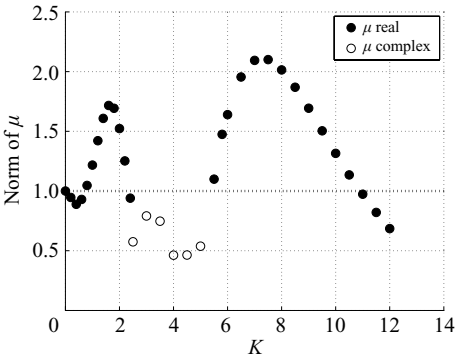

FIGURE 2. Norm of the Floquet multiplier μ as a function of the wavenumber k at $Re = 300$ obtained on the grid GRC.

case of the unconfined circular cylinder (Giannetti & Luchini 2007; Luchini *et al.* 2008; Giannetti *et al.* 2009) and of a confined square cylinder (Camarri & Giannetti 2007).

3. Results and discussion

A computational domain has been chosen with $L_i = 12.5\ D$ and $L_o = 35.5\ D$, which is similar to the ones selected in other studies on the same flow documented in the literature (see for instance Chen *et al.* 1995; Zovatto & Pedrizzetti 2001). Two stretched Cartesian grids have been used in the present study. The coarser one (GRC) has 495 (N_x) and 196 (N_y) points in the x and the y direction, respectively, with a resolution varying from ($\Delta x_{min} = 1.3 \times 10^{-2}\ D$, $\Delta y_{min} = 1.7 \times 10^{-2}\ D$) on the body to ($\Delta x_{max} = 2.2 \times 10^{-1}\ D$, $\Delta y_{max} = 6.2 \times 10^{-2}\ D$) at the outflow boundary. The finer grid (GRR) is obtained by increasing the resolution near the body and in the far wake, and it is characterized by $N_x = 660$, $N_y = 280$, $\Delta x_{min} = 1.1 \times 10^{-2}\ D$, $\Delta y_{min} = 1.4 \times 10^{-2}$, $\Delta x_{max} = 1.9 \times 10^{-1}\ D$ and $\Delta y_{max} = 3.0 \times 10^{-2}\ D$. The grid resolution of GRR on the cylinder and in the near wake is very similar to that used in Giannetti *et al.* (2009) for the Floquet stability analysis of the unconfined case, for which the present numerical tools are shown to provide results in very good agreement with the literature. As for the temporal discretization, $\Delta t \simeq 1 \times 10^{-2} D/U_c$ and $\Delta t \simeq 8.5 \times 10^{-3} D/U_c$ have been used with GRC and GRR, respectively. For a further validation of the numerical tools and the grids used, a simulation was carried out at $Re = 300$, which is larger than the values of interest for the present study, and the resulting Strouhal numbers ($St = f\ D/U_c$, f being the vortex-shedding frequency), equal to $St \simeq 0.2036$ and $St \simeq 0.2032$ for grids GRC and GRR, respectively, are in good agreement with the value $St \simeq 0.199$ obtained in Zovatto & Pedrizzetti (2001) and indicate grid convergence for St.

As a first analysis, the norm of the dominant Floquet multiplier has been evaluated as a function of the wavenumber k of the disturbance at $Re = 300$ using the grid GRC; the results are reported in figure 2. All the unstable multipliers are real and there are two clearly separated bands of unstable modes, centred at $k \simeq 1.3$ and at $k \simeq 7$. The band of modes centred at $k \simeq 1.3$ first becomes unstable at a critical wavenumber $k_A \simeq 1.35$ and at a critical Reynolds number Re_A. Using grids GRC and GRR, we estimated $Re_A \simeq 201.2$ and $Re_A \simeq 200.5$, respectively. At $Re = 201$ the Strouhal number changes only at the fourth decimal unit in passing from grid GRC to grid GRR, its value being $St \simeq 0.193$. An analysis of the space–time symmetries of

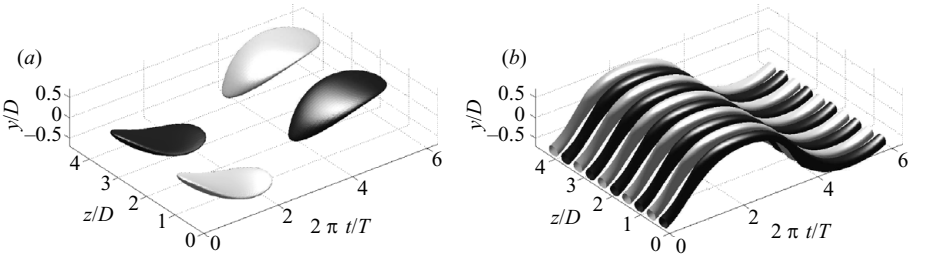

FIGURE 3. Space–time reconstruction of streamwise vorticity $\omega_x(x, y, z, t)$ passing in time through the section $x = 2D$ (grid GRR) for (a) mode A ($k = 1.35$, $Re = 204$) and (b) mode B ($k = 7.325$, $Re = 256$); dark and light colours indicate negative and positive values, respectively.

the unstable mode at ($k = 1.35$, $Re = 204$) using grid GRR reveals that this mode and the band of unstable modes centred around $k \simeq 1.3$ have the same symmetries of the mode A in the unconfined case, i.e.

$$\hat{u}(x, y, k, t) = \hat{u}(x, -y, k, t + T/2), \tag{3.1a}$$

$$\hat{v}(x, y, k, t) = -\hat{v}(x, -y, k, t + T/2), \tag{3.1b}$$

$$\hat{w}(x, y, k, t) = \hat{w}(x, -y, k, t + T/2), \tag{3.1c}$$

in which $\hat{u}$, $\hat{v}$, $\hat{w}$ are the x, y and z components of the disturbance velocity $\hat{\boldsymbol{u}}$ and T is the period of the two-dimensional base flow. Consequently, the axial vorticity $\hat{\omega}_x$ of the field $\hat{\boldsymbol{u}}$ is characterized by the symmetry $\hat{\omega}_x(x, y, k, t) = -\hat{\omega}_x(x, -y, k, t + T/2)$. This is confirmed by the space–time reconstruction of the axial vorticity measured at section $x = 2D$, which is plotted in figure 3(a). For this reason we will denote the transition to a three-dimensional state due to the considered band of unstable modes as 'mode A'. The symmetry of mode A is physically explained in Williamson (1996) as the result of a self-sustaining formation of vortex loops at particular spanwise locations due to the induction of one vortex loop on a newly forming primary vortex. Note that this interpretation is also compatible with the inverted arrangement of the wake vortices of the considered case. Besides symmetries, the wavelength in the spanwise direction of the critical mode, $\lambda_A/D = 2\pi/k_A \simeq 4.65$, is quantitatively comparable to what is observed experimentally in Williamson (1996) and to what is found numerically for mode A in the unconfined case in Barkley & Henderson (1996) ($\lambda/D = 3.96 \pm 0.02$). Lastly, although there is a variable inflow velocity profile here and we arbitrarily based the Reynolds number on U_c (see figure 1), the critical Reynolds number for mode A so obtained is similar to the one found in Barkley & Henderson (1996) for the unconfined case ($Re \simeq 188.5 \pm 1$). Summarizing, the analysis of the space–time symmetries shows that the transition involving modes around $k = 1.3$ is identical to what is observed in the unconfined case for mode A. Nevertheless, the shape of the linear unstable modes is inevitably influenced by the convection caused by the two-dimensional (time periodic) base flow. In this connection there is a difference between the confined and the unconfined cases due to the inversion of the wake vortices. This is highlighted in figure 4, where the streamwise vorticity of mode A is plotted toghether with the spanwise vorticity of the base flow for the confined (figure 4a) and the unconfined (figure 4b) case (this has been computed with $Re = 190$ and $k = 1.585$; details are given in Giannetti *et al.* 2009). The comparison between figures 4(a) and 4(b) clearly shows how the base flow and, in particular, the inversion of the wake vortices, affects the shape of the unstable linear mode. Details of the distribution of

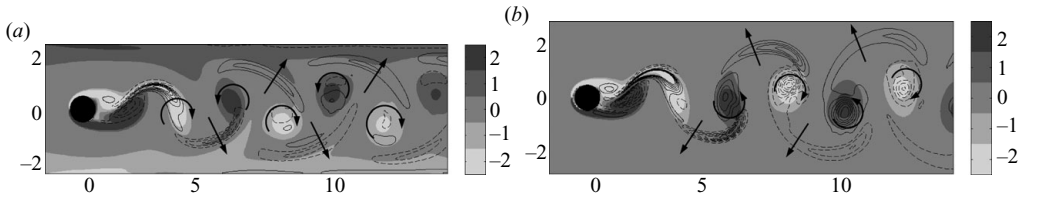

FIGURE 4. Detailed views of the spanwise vorticity (coloured plot) of the two-dimensional base flow and contours of the streamwise vorticity (dotted lines stand for negative values) of mode A in the confined (*a*) and unconfined (*b*) case. The straight arrows indicate the direction of the velocity induced by the von Kármán wake vortices of the two-dimensional flow, whose position and sense of rotation is represented by the circular arrows.

axial vorticity of mode A in figure 4(*b*) are in good agreement with those shown in Thompson *et al.* (2001) and with the flow visualizations in Williamson (1996).

As regards the second band of unstable modes, centred around $k \simeq 7$ (see figure 2), this becomes unstable at a critical wavenumber $k_B \simeq 7.325$ and at a critical Reynolds number Re_B, which is found to be equal to $Re_B \simeq 257.0$ and $Re_B \simeq 255.7$ using grids GRC and GRR, respectively. At $Re = 256.7$ the Strouhal number is $St \simeq 0.199$ and changes only at the fourth decimal digit in passing from GRC to GRR. For this band of modes a different space–time symmetry is found, which is identical to the mode B type of transition of the unconfined case:

$$\hat{u}(x, y, k, t) = -\hat{u}(x, -y, k, t + T/2), \tag{3.2a}$$

$$\hat{v}(x, y, k, t) = \hat{v}(x, -y, k, t + T/2), \tag{3.2b}$$

$$\hat{w}(x, y, k, t) = -\hat{w}(x, -y, k, t + T/2), \tag{3.2c}$$

$$\hat{\omega}_x(x, y, k, t) = \hat{\omega}_x(x, -y, k, t + T/2). \tag{3.2d}$$

This is shown in figure 3(*b*) by plotting a space–time reconstruction of the axial vorticity passing at section $x = 2D$. We will denote the transition to a three-dimensional state due to the considered band of unstable modes as 'mode B' for its space–time symmetries. A physical interpretation of the symmetry of mode B is given in Williamson (1996) showing that the axial vorticity on an existing braid shear layer induces spanwise perturbations on a newly forming braid shear layer which respect the symmetry of mode B. This interpretation remains compatible with the position of the braid shear layers found here due to the inverted wake vortices. As in the previous case, the critical wavelength in the spanwise direction, $\lambda_B/D \simeq 0.86$, and the critical Reynolds number, $Re_B \simeq 255.7$, are quantitatively very similar to the corresponding ones in the unconfined case, which are equal to $\lambda/D \simeq 0.82$ and to $Re = 259 \pm 2$ (Barkley & Henderson 1996), respectively. Nevertheless, the inversion of the wake vortices affects the shape of the unstable linear mode B in the same way as that in which it influences the shape of mode A (not reported here for the sake of brevity).

Summarizing, the transition of the wake to a three-dimensional state for the confined flow considered here is identical to that of the unconfined case, at least in the explored range of Re ($\leqslant 300$) and k ($\leqslant 12$), although the two base flows are significantly different due to the inversion of the von Kármán wake vortices. However, the different arrangement of the wake vortices leads to different instantaneous shapes of the linear modes, which are inevitably influenced by the convection caused by the two-dimensional base flow. A possible interpretation of this result is now proposed;

it is based on the observation that, at least in the unconfined case, the region of the base flow that is responsible for the three-dimensional instability of the wake, which we will denote as the core of the instability, is sharply localized in the near-wake region. This region has been identified with a combined analysis of the unstable Floquet modes and of their adjoint modes in Luchini *et al.* (2008) and in Giannetti *et al.* (2009), generalizing the work documented in Giannetti & Luchini (2007) to include the case of a periodic base flow. Previously, the same region was heuristically identified in Barkley (2005) where, by carrying out Floquet stability analyses on progressively smaller domains, it is shown that only 'small regions of the full flow just behind the cylinder are responsible for the linear instabilities despite the fact that the actual linear modes extend many cylinder diameters downstream the cylinder'. Quantitatively, in Luchini *et al.* (2008) and in Giannetti *et al.* (2009) it is shown that the core of the three-dimensional instability is contained in a region $-0.5D < x < 2.5$, $-D < y < D$ (same frame of reference sketched in figure 1), while mode B is localized slightly closer to the cylinder downwind face than mode A. This information on the core of the instability suggests the following interpretation of the present results: the three-dimensional instability originates in a flow region in which the wake vortices are in a developing stage and, thus, where inversion has not yet taken place. This might explain the similarity with the unconfined case. Naturally, the base flow affects the shape of the unstable modes further downstream.

In order to support this interpretation, the core of the three-dimensional instability has been localized in the considered case. In this connection we have followed the approach proposed in Luchini *et al.* (2008) and in Giannetti *et al.* (2009), which is now briefly recalled, and the results have been verified by carrying out Floquet analyses on progressively smaller computational domains, as done in Barkley (2005). To identify the core of the instability, a localized structural perturbation to the linearized momentum equation (2.1a) is considered. In particular, indicating with LHS the left-hand side of equation (2.1a), the considered structural perturbation has the following form:

$$\mathrm{LHS} = \delta(x - x_0, y - y_0)\boldsymbol{C}_0 \cdot \hat{\boldsymbol{u}}, \tag{3.3}$$

where $\boldsymbol{C}_0$ is a generic constant (feedback) matrix, the symbol '$\cdot$' stands for matrix vector product, (x_0, y_0) are the coordinates of the point where the feedback acts and $\delta(x, y)$ denotes the Dirac delta function. By carrying out a perturbation analysis of the variation of the eigenvalue σ caused by the structural perturbation (3.3), using the properties of the adjoint velocity field $\boldsymbol{f}^+$, we obtain that $\delta\sigma = \boldsymbol{C}_0 : \boldsymbol{S}(x_0, y_0, k)$ where the symbol ':' stands for double contraction of the indices and $\boldsymbol{S}$ is the sensitivity tensor of the Floquet mode:

$$\boldsymbol{S}(x, y, k) = \frac{\displaystyle\int_t^{t+T} \hat{\boldsymbol{f}}^+(x, y, \kappa, t)\, \hat{\boldsymbol{u}}(x, y, \kappa, t)\, \mathrm{d}t}{\displaystyle\int_t^{t+T} \int_{\mathscr{D}} \hat{\boldsymbol{f}}^+ \cdot \hat{\boldsymbol{u}}\, \mathrm{d}S\, \mathrm{d}t}. \tag{3.4}$$

Note that this definition is independent of the particular feedback matrix $\boldsymbol{C}_0$. The region of the flow field in which the instability mechanism arises coincides with the region where the norm of $\boldsymbol{S}$ is significantly different from zero. The spectral norm has been used here (i.e. the maximum eigenvalue of $\boldsymbol{S}^{\boldsymbol{H}}\boldsymbol{S}$, $\boldsymbol{S}^{\boldsymbol{H}}$ being the conjugate transpose of $\boldsymbol{S}$), but different norms lead to very similar results. The quantity $\|\boldsymbol{S}(x, y, \kappa)\|$ is plotted in figure 5, which shows that the core of the instability for both modes A and B is sharply localized in the near wake. Moreover, the quantitative similarity with

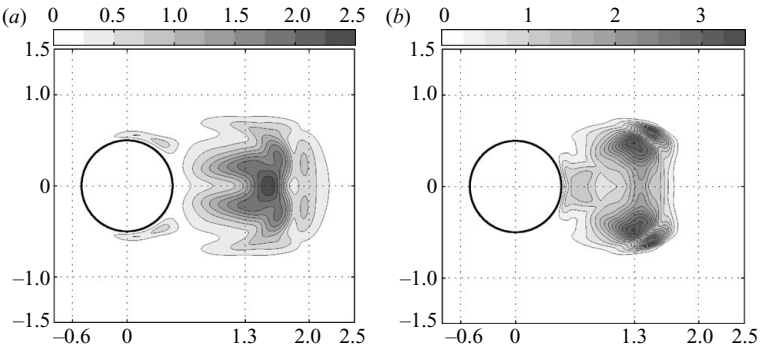

FIGURE 5. Spectral norm of the tensor field $\boldsymbol{S}$ at each point of the domain for (a) mode A ($Re = 201$, $k = 1.35$) and (b) mode B ($Re = 256.7$, $k = 7.325$) obtained on grid GRR.

the corresponding figures in the unconfined case reported in Giannetti *et al.* (2009) is striking.

The statement that only the regions where $\|\boldsymbol{S}(x, y, \kappa)\|$ is significantly different from zero are important for the instability mechanism has been verified *a posteriori* by carrying out Floquet stability analyses on progressively smaller rectangular subdomains around that region. The Floquet multipliers obtained in the subdomains are then compared to the reference one obtained on the whole domain. To this purpose, the considered base flow is always the one computed on the whole domain and, in restricting it to subdomains, the grid points are left unchanged in order to avoid interpolation errors. The boundary conditions on each side of the subdomains are identical to those imposed on the corresponding side of the whole domain. In a sense, the strategy proposed in Giannetti *et al.* (2009) has been used here only to quickly localize this region, so avoiding a trial-and-error procedure. As an example, we report here the results obtained for mode B at incipient instability. In this case we considered three subdomains: (i) ($-0.6D \leqslant x \leqslant 2.5D$, $-1.5D \leqslant y \leqslant 1.5D$), (ii) ($-0.6D \leqslant x \leqslant 2.0D$, $-D \leqslant y \leqslant D$) and (iii) ($-0.6D \leqslant x \leqslant 1.3D$, $-D \leqslant y \leqslant D$). For the sake of clarity, some grid lines in figure 5(b) correspond to the boundaries of the listed subdomains. The figure shows that, while (i) and (ii) contain the region where $\|\boldsymbol{S}(x, y, \kappa)\|$ is significantly non-null, (iii) does not. Passing progressively from (i) to (iii) the Floquet multipliers obtained are $\mu = 1.0215$, $\mu = 0.9738$, $\mu = 2.883$, while the reference one obtained on the whole computational domain is $\mu = 1.0214$ (the relative percentage variations being approximately equal to 0.8 %, −4.7 % and 182 %, respectively). The same analysis has been carried out for mode A (results are not reported, for the sake of brevity), so validating the region identified in figure 5(a).

To support the interpretation of the results proposed above, the same isocontours of $\|\boldsymbol{S}(x, y, \kappa)\|$ reported in figure 5 have been plotted so as to overlap with the vorticity field of the base flows of mode A and B in figure 6. For both modes the resulting pictures clearly show that, in the region where $\|\boldsymbol{S}(x, y, \kappa)\|$ is significantly non-null, the wake vortices are still in a developing stage and, thus, it is not even possible to speak about their inversion in that region. In particular, according to our analysis, mode A and mode B type of transitions would be affected by the confinement only if its effects would change the base flow in the region where the wake vortices form, which is evidently upstream with respect to their subsequent inversion. Acting only on the blockage ratio, this effect is expected only for a large confinement. For instance, the experiments by Rehimi *et al.* (2008) show that the nature of three-dimensional

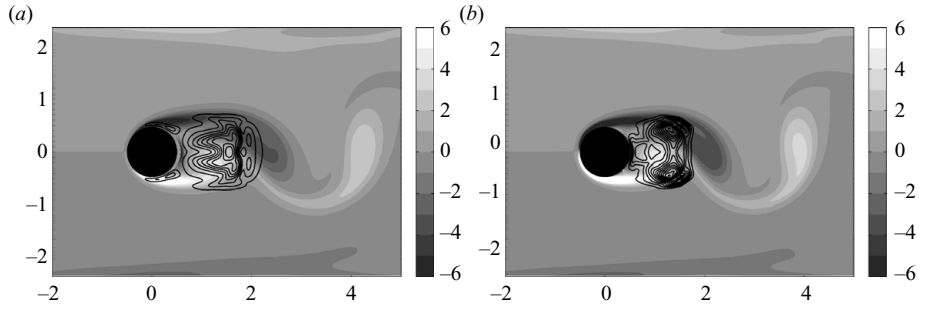

FIGURE 6. Spectral norm of the tensor field $\boldsymbol{S}$ (same isolines as in figure 5) and vorticity field (grey-scale contours) of the base flow for (*a*) mode A ($Re = 201$, $k = 1.35$) and (*b*) mode B ($Re = 256.7$, $k = 7.325$) obtained on grid GRR.

transition is substantially unchanged with respect to the unconfined case also at $\beta = 1/3$. This is confirmed by a Floquet stability analysis that we carried out for the same case (not reported here) which confirms what is documented in the present paper for $\beta = 1/5$. However, we wish to remark that, as the blockage ratio is further increased, new unstable modes might appear and eventually become dominant in the transition to the three-dimensional state.

As a final element to support the interpretation of the results given above, we provide the following quantitative measurement of the similarity between the confined and the unconfined two-dimensional flows in the region identified as the core of the three-dimensional instability. A weighted spatial correlation coefficient has been defined between the vorticity fields of the confined (Ω_c) and the unconfined (Ω_u) case corresponding to the same phase of the vortex shedding cycle:

$$C = \frac{\int_V \Omega_c \; f_w \; \Omega_u \mathrm{d}V}{\sqrt{\int_V f_w \; \Omega_c^2 \mathrm{d}V}\sqrt{\int_V f_w \; \Omega_u^2 \, \mathrm{d}V}}, \tag{3.5}$$

where f_w is a generic (non-negative) weighting function and V is the overlapping region between the computational domains of the two cases, starting from $x = -0.5D$ (in order to exclude the inflow region which is not interesting) and ending at $x = 30D$. In a first case (C_1) we considered $f_w = f_{w1}$, where f_{w1} is the pointwise maximum between the norms of the sensitivity tensors ($\boldsymbol{S}$) of the confined and the unconfined case. Conversely, in a second case (C_2) we considered $f_w = f_{w2}$, where f_{w2} is equal to 1 where $f_{w1} < 10^{-2} \max(f_{w1})$ and 0 otherwise, thus being a kind of complementary weight to f_{w1}. The resulting correlation coefficients have been averaged in time using 20 instantaneous flow fields equispaced on a vortex shedding cycle for mode A (the two cases documented in figure 4 have been considered). As a result $C_1 \simeq 0.987$, so showing a high degree of similarity of the two flows in the core of the three-dimensional instability, which coincides with the vortex formation region. Conversely, $C_2 \simeq 0.296$, demonstrating that the two wakes are poorly correlated in terms of vorticity distribution outside the core of the instability. Spatial information on the similarity between the two vorticity fields has been derived by evaluating their correlation in time, averaged on one vortex shedding period. The result is reported in figure 7, which shows that, close to the cylinder in the downstream region, the time histories of the two vorticity fields are very similar, their correlation being larger

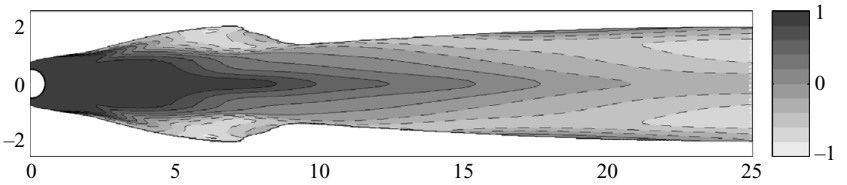

FIGURE 7. Correlation in time between the vorticity of the two-dimensional base flows of the confined and unconfined case in the critical conditions of mode A instability; regions of low vorticity of the unconfined case have been eliminated (lateral white bands).

than 0.9. Conversely, the correlation becomes negative further downstream, due to the inversion of the wake vortices in the confined case.

4. Conclusions

In the present work the three-dimensional stability of the wake of a moderately confined circular cylinder has been investigated by a linear stability analysis and both mode A and mode B three-dimensional instabilities have been observed. The associated critical wavelengths and Reynolds numbers are also quantitatively similar to those found for the unconfined case. However, the instantaneous shape of the linear modes is different, due to the different arrangement of the vortices in the wake. A possible interpretation of this result is proposed, according to which the inversion of the wake vortices does not affect the nature of the instability because its core is sharply localized in the near-wake region, where the wake vortices are still forming. The proposed interpretation is supported by the localization of the core of the instability for both modes A and B, carried out using a technique based on the combined analysis of the direct and adjoint unstable modes; the resulting regions have been then verified *a posteriori*. The experiments by Rehimi *et al.* (2008) and our numerical investigation suggest that the conclusions drawn in the present paper are valid at least for blockage ratios up to $\beta = 1/3$. Indeed, the core of the modes A and B is so close to the cylinder rear face that only an even larger blockage ratio is expected to influence the flow in that region. However, as β is further increased, the flow soon experiences significant changes and thus the comparison with the unconfined case becomes less interesting; as an example, in Sahin & Owens (2004) it is shown that, already for $\beta \simeq 1/2$, the base flow is sensibly different with respect to the unconfined case, and vortices are shed both from the body and from the confining walls.

The authors are grateful to Professor P. Luchini for his scientific support; the simulations were carried out thanks to the computational resources of DIMEC (Salerno).

REFERENCES

BARKLEY, D. 2005 Confined three-dimensional stability analysis of the cylinder wake. *Phys. Rev.* E **71**, 017301.

BARKLEY, D. & HENDERSON, R. D. 1996 Three-dimensional Floquet stability analysis of the wake of a circular cylinder. *J. Fluid Mech.* **322**, 215–241.

BUFFONI, M., CAMARRI, S., IOLLO, A. & SALVETTI, M. V. 2006 Low-dimensional modelling of a confined three-dimensional wake flow. *J. Fluid Mech.* **569**, 141–150.

CAMARRI, S. & GIANNETTI, F. 2007 On the inversion of the Kármán street in the wake of a confined square cylinder. *J. Fluid Mech.* **574**, 169–178.

Chen, J.-H., Pritchard, W. G. & Tavener, S. J. 1995 Bifurcation for flow past a cylinder between planes. *J. Fluid Mech.* **284**, 23–41.

Giannetti, F., Camarri, S. & Luchini, P. 2009 Structural sensitivity of the secondary instability in the wake of a circular cylinder. Manuscript submitted for publication.

Giannetti, F. & Luchini, P. 2007 Structural sensitivity of the first instability of the cylinder wake. *J. Fluid Mech.* **581**, 167–197.

Luchini, P., Giannetti, F. & Pralits, J. 2008 Structural sensitivity of linear and nonlinear global modes. In *Fifth AIAA Theoretical Fluid Mechanics Conference*, paper no. AIAA–2008–4227. Seattle, WA, June 23–26.

Noack, B. R. & Eckelmann, H. 1994 A global stability analysis of the steady and periodic cylinder wake. *J. Fluid Mech.* **270**, 297–330.

Rehimi, F., Aloui, F., Nasrallah, S. B., Doubliez, L. & Legrand, J. 2008 Experimental investigation of a confined flow downstream of a circular cylinder centred between two parallel walls. *J. Fluids Struct.* **24** (6), 885–882.

Sahin, M. & Owens, R. G. 2004 A numerical investigation of wall effects up to high blockage ratios on two-dimensional flow past a confined circular cylinder. *Phys. Fluids* **16** (5), 1305–1320.

Suzuki, H., Inoue, Y., Nishimura, T., Fukutani, K. & Suzuki, K. 1993 Unsteady flow in a channel obstructed by a square rod (crisscross motion of vortex). *Int. J. Heat Fluid Flow* **14** (1), 2–9.

Thompson, M. C., Leweke, T. & Williamson, C. H. K. 2001 The phyisical mechanism of transition in bluff body wakes. *J. Fluids Struct.* **15**, 607–616.

Williamson, C. H. K. 1988 The existence of two stages in the transition to three-dimensionality of a cylinder wake. *Phys. Fluids* **31** (11), 3165–3168.

Williamson, C. H. K. 1996 Three-dimensional wake transition. *J. Fluid Mech.* **328**, 345–407.

Zovatto, L. & Pedrizzetti, G. 2001 Flow about a circular cylinder between parallel walls. *J. Fluid Mech.* **440**, 1–25.